LA-UR- 97-2461

Approved for public release; distribution is unlimited.

Title: Low-noise detector and amplifier design for 100 ns direct detection CO2 LIDAR receiver

CONF-970706--

Author(s): Maureen M. Cafferty NIS-4
Bradly Cooke NIS-4
Bryan E. Laubscher NIS-4
Nicholas L. Olivas NIS-4
Kenneth Fuller NIS-4

Submitted to: San Diego SPIE conference, July 1997

Los Alamos
NATIONAL LABORATORY

DISCLAIMER

Low-noise detector and amplifier design for 100 ns direct detection CO_2 LIDAR receiver

M. M. Cafferty, B. J. Cooke, B. E. Laubscher, N. L. Olivas, K. Fuller
Los Alamos National Laboratory, MS-D448, Los Alamos, NM 87545

ABSTRACT

The development and test results of a prototype detector/amplifier design for a background limited, pulsed 100 ns, 10-100 kHz repetition rate LIDAR/DIAL receiver system are presented. Design objectives include near-matched filter detection of received pulse amplitude and round trip time-of-flight, and the elimination of excess correlated detector/amplifier noise for optimal pulse averaging. A novel pole-zero cancellation amplifier, coupled with a state-of-the-art SBRC (Santa Barbara Research Center) infrared detector was implemented to meet design objectives.

The pole-zero cancellation amplifier utilizes a tunable, pseudo-matched filter technique to match the width of the laser pulse to the shaping time of the filter for optimal SNR performance. Low frequency correlated noise, (1/f and drift noise) is rejected through a second order high gain feedback loop. The amplifier also employs an active detector bias stage minimizing detector drift.

Experimental results will be provided that demonstrate near-background limited, 100 ns pulse detection performance given a 8.5-11.5 μm (300 K B.B.) radiant background, with the total noise floor spectrally white for optimal pulse averaging efficiency.

Keywords: IR receiver, pseudo-matched filter, correlated noise

1. INTRODUCTION

1.1 Receiver design requirements

- dynamic range of 60 dB
- pseudo-matched filter detection of 100ns wide optical pulse, bandwidth of ~5 MHz
- pulse repetition rate (PRR) of 10 kHz-100 kHz
- system noise below background (300 K), noise equivalent power (NEP)=0.3 nW, input noise current i_n<1.6 nA rms
- 60° Field of view (FOV)
- remove or minimize drift and low frequency correlated noise, (1/f)

In addition, the detector requirements submitted to the vendor are as follows:

- 200 μm square detector (could be circular)
- Optical bandwidth: 8-12 μm
- Quantum efficiency: >65% over $\Delta\lambda$ = 9-11.5 μm
- I_d<100 nA @ 50-100 mV reverse bias
- R_d>500 kΩ @ 50-100 mV reverse bias
- C_d~10 pF @ 50-100 mV reverse bias
- Bandwidth: >20 MHz

The detector must be cryogenically cooled below liquid nitrogen (77 K) utilizing liquid helium or a mechanical cooler. The optimal operating temperature for the detector is determined from spectral IR measurements to measure the cutoff wavelength as a function of temperature. The wide bandwidth, high gain, low noise requirements dictate that the front-end electronics be no more than a few centimeters away from the detector. Therefore, a portion of the preamplifier must

be mounted inside the dewar with the detector. The system also requires relatively low power for battery operation up to 16 hours.

2. DESIGN

2.1 Preamplifier/amplifier component choices

The most important parameters driving the choice of components are low noise, low power, dynamic range, and bandwidth. The largest contributions to noise are from the detector and the front-end electronics. To limit the current noise contribution from the front-end electronics, a cooled JFET is used at the input of the preamplifier. The JFET will be cooled inside the dewar along with the detector, but the JFET and associated parts must be kept at or above 120 K for optimal noise performance. The components that must be mounted inside the dewar with the detector for low noise operation are; the JFET, the feedback resistor and capacitor, and part of the detector bias circuitry. These components must be mounted on a separate board from the detector so the thermal coupling to the detector is minimal. It is very important to note that the detector must be maintained at a stable temperature between 25 K and 50 K, the electronics must be at or above 120 K, and the distance between them kept short, (a few centimeters at most).

Several possible candidates for the JFET were chosen based on their high transconductance and low capacitance. The ratio of transconductance to capacitance is an important figure of merit in choosing a JFET. A higher figure is better. The transconductance was measured for several of each of three different types of JFETs, (2SK443, 2SK152, and 2SK715) and the most consistent type was chosen, 2SK715.

The opamp requirements limit the choice severely. The final choice of the CLC426 was determined by its low-noise, high bandwidth (full power bandwidth), high gain range, adjustable supply current capability, and high output swing at +/-5 V supplies. The baseline restorer requirements are minimal. It requires low power and stability at unity gain.

2.2 Summary of detector/amplifier noise sources

2.2.1 Detector

An in-depth detailed analysis is given in **Reference 1 and 2**. A simplified analysis of the detector noise gives the primary noise sources as Johnson, shot, 1/f, temperature, and microphonics. The total noise is the quadrature sum of all noise sources. In the following equations, the variables are defined as: i is the current noise, k is Boltzmann's constant, T is the temperature in Kelvin, Δf is the bandwidth, R is the detector resistance, A_d is the detector area, and q is charge.

Johnson noise current is given as:

$$i_j = \sqrt{\frac{4 \cdot k \cdot T \cdot \Delta f}{R}} \tag{1}$$

This equation shows that as the detector resistance is increased, the noise current decreases, therefore the detector resistance should be made as large as possible. The noise current is also related to the detector active area. The resistance-detector -area product (RA_d) can be shown to be a constant. If this is substituted in the above equation, then the equation becomes:

$$i_j = \sqrt{\frac{4 \cdot k \cdot T \cdot \Delta f}{(RA_d)} \cdot A_d} \tag{2}$$

This shows the noise increasing proportionally with the square root of the active area of the detector.

Shot noise current is given as:

$$i_s = \sqrt{2 \cdot q \cdot I \cdot \Delta f} \tag{3}$$

The I in the equation can be photocurrent or dc current or both. Assuming photocurrent is negligible when the detector is blocked from optical sources, then the dc leakage current will dominate. The dc current is proportional to the cross-sectional area of the active detector, therefore the noise is also proportional to the square root of the detector area. The detector area should be as small as is possible within system FOV constraints described in **Reference 6**.

A nonstationary noise component that tends to be present in most photoconductors and active devices is 1/f noise. Typically, 1/f noise power is proportional to the square of the current and falls off as f^b, $0.5 \le b \le 2$. It is associated with dc current. In the following equation, K is a constant for a given device, I_D is the drain bias current, and f is the frequency. The spectral density equation is[3]:

$$i = \sqrt{K \frac{I_D^2}{f^b}} \quad [A/\sqrt{Hz}] \tag{4}$$

Temperature noise is the temperature fluctuation of the sensitive element. The causes include radiative exchange with the surroundings and/or conductance with the cold finger. The temperature of the detector has a mean value, but some fluctuation is associated with it. To minimize this noise, the detector temperature and surroundings must be very stable

Microphonic noise is caused by mechanical displacement. The noise results from changes in the interelectrode wire capacitance caused by displacement relative to ground. Vibrations at the detector must be minimized to reduce this noise.

2.2.2 Amplifier

2.2.2.1 JFET/Preamplifier

Most of the noise contribution from the amplifier section is from the front-end transistor and the feedback resistor. The current noise due to the feedback resistor R_f is:

$$i = \sqrt{\frac{4 \cdot k \cdot T \cdot \Delta f}{R_f}} \tag{5}$$

Therefore, the feedback resistor should be made as large as possible, but other consequences of a large R_f must be considered, for example, the decay time of C_fR_f (this affects the maximum PRR due to pulse pileup), and DC offset from the bias current of the detector or preamplifier input current. Solutions to this problem include AC coupling the detector and using a JFET at the input of the preamplifier because of its very small gate current (pA).

The current noise from the JFET is small for large source impedances and the noise decreases with temperature until about 120 K. At about this temperature, the noise contribution from the JFET increases with decreasing temperature. The noise is a strong function of the transconductance to input capacitance ratio. The noise decreases as this number increases. This can be shown in the following current spectral density equation with the variables defined as follows, C_{gs} is the JFET gate to source impedance, g_m is the transconductance, and C_s is the source capacitance:

$$i(f) = \sqrt{\left[\frac{(2 \cdot \pi \cdot f)^2 \cdot (C_{gs})^2}{g_m^2} \cdot \left(4 \cdot k \cdot T \cdot \frac{2}{3} \cdot g_m\right) + \left[4 \cdot k \cdot T \cdot \left(\frac{2}{3 \cdot g_m}\right) \cdot \left[2 \cdot \pi \cdot f \cdot \left(C_s + C_{gs}\right)\right]^2 + \frac{4 \cdot k \cdot T}{R_f}\right]\right]} \quad [A/\sqrt{Hz}] \tag{6}$$

This equation can be used for an initial estimate of the current noise contribution from the JFET due to the source impedance and the feedback impedance. The dependencies on g_m and the source impedance are very evident here. Note that this is not the complete current noise equation for the JFET[3,4].

An active baseline restoration circuit implemented in the preamplifier feedback loop rejects low frequency drift noise.

2.2.2.2 Matched Filter

A derivation of the matched filter technique can be found in **Reference 5**. Put simply, the filter should attenuate strongly those frequencies that have little signal energy and attenuate very little the frequencies that have strong signal energy. In reality, an exact matched filter in unrealizable, but an nth order low-pass filter with the same bandwidth as the signal can be designed very simply for our system[6]. A passive filter (RLC) matched to 100 ns pulses was implemented in this design and a preliminary design for an electronically tunable filter was developed.

The electronically tunable filter[7] design is shown in **Figure 1**. The design, which was prototyped and tested, is a two-pole filter with a tunable range of 27 db.

A description of the voltage controlled filter follows. The transfer function for the AD835 multiplier in **Figure 1** is:

$$V_{outn} = \frac{(X1 - X2)(Y1 - Y2)}{1 \cdot Volt} + Z \tag{7}$$

With the following substitutions,

$$Y1a = Vin,\ X2 = 0,\ Y2a = Za = Vinb,\ Y2b = Zb = Vout$$

$$Vouta = X1(Vin - Vinb) + Vinb \qquad Voutb = X1(Vinb - Vout) + Vout$$

$$Vinb = Vouta\left(\frac{1}{s \cdot C \cdot R + 1}\right) \qquad Vout = Voutb\left(\frac{1}{s \cdot C \cdot R + 1}\right) \tag{8}$$

$$\varpi_o = \frac{1}{C \cdot R} \qquad f_o = \frac{1}{2 \cdot \pi \cdot C \cdot R}$$

The final equation is:

$$Vout = \frac{Vinb}{1 + \frac{s \cdot C \cdot R}{X1}} = \frac{Vin}{\left(1 + \frac{s \cdot C \cdot R}{X1}\right)^2} = \frac{Vin}{\left(1 + \frac{j \cdot 2 \cdot \pi \cdot f}{2 \cdot \pi \cdot f \cdot X1}\right)^2} \tag{9}$$

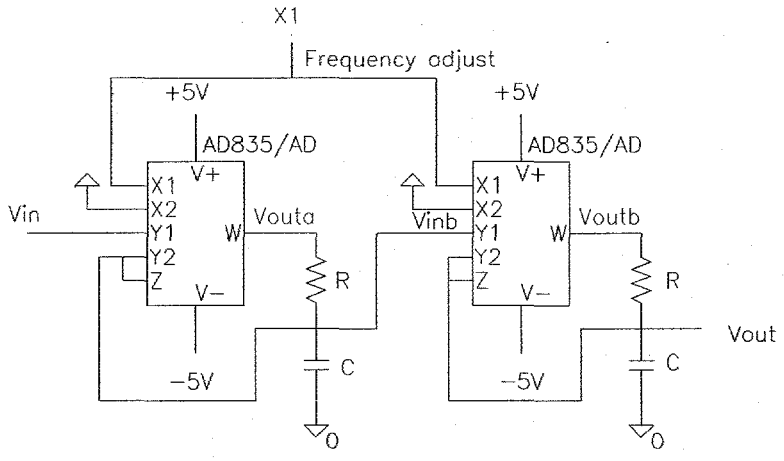

Figure 1
Schematic for voltage controlled filter

2.3 Spice simulation of the amplifier

The design of the amplifier is shown in **Figure 2** and **Figure 3**. The first section (**Figure 2**) shows the active detector bias circuit, the preamplifier, the 1/f low pass filter, and the pole-zero compensation components. The second section (**Figure 3**) shows the gain and matched filter stages along with the baseline restorer.

The active detector bias sinks the dark current plus photocurrent and is capable of sinking up to 20 μA of photocurrent. The AC signal current which is passed by the active bias circuit is integrated at the preamplifier. A pole-zero (integrate-derivative) cancellation approach is implemented so that R_f can be made very large reducing the noise floor. An integrator (pole) is formed with C_f, producing an integration time-constant of $\tau_o = R_f C_f$ thereby limiting the bandwidth to $1/2\pi\tau_o$. This loss in bandwidth is then restored through a derivative (zero) operation with a time constant of τ_o. Hence, the reduced noise advantage of a large R_f can be preserved without loss of AC bandwidth[5].

The electronic filter, h(t), is selected so as to closely match receiver to signal bandwidth, optimizing the signal to noise performance. Here, the filter is matched to a 100 ns pulse, about 5 MHz.

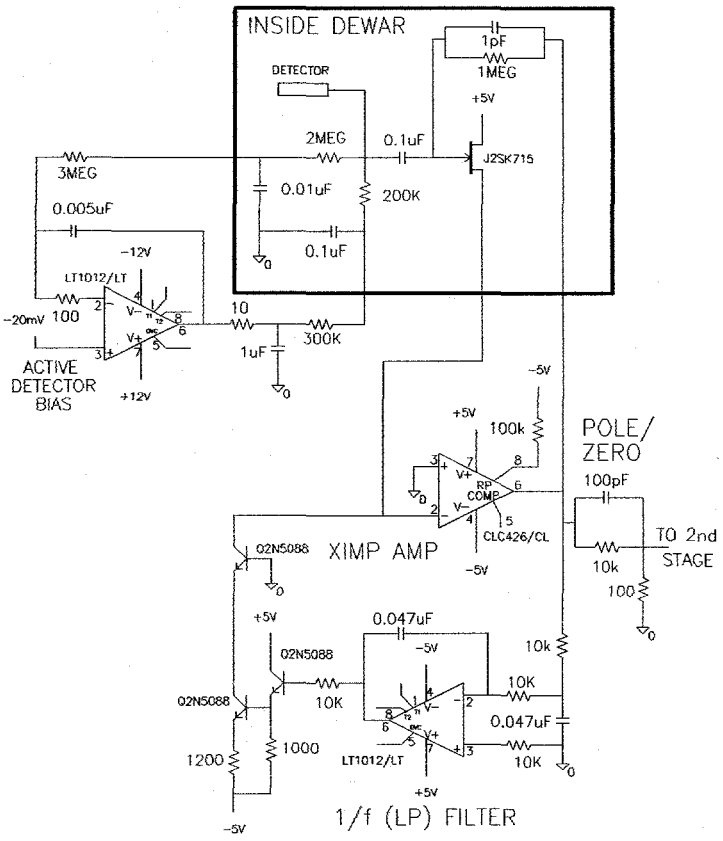

Figure 2
Active detector bias, preamplifier and 1/f filter, and cooled front-end electronics

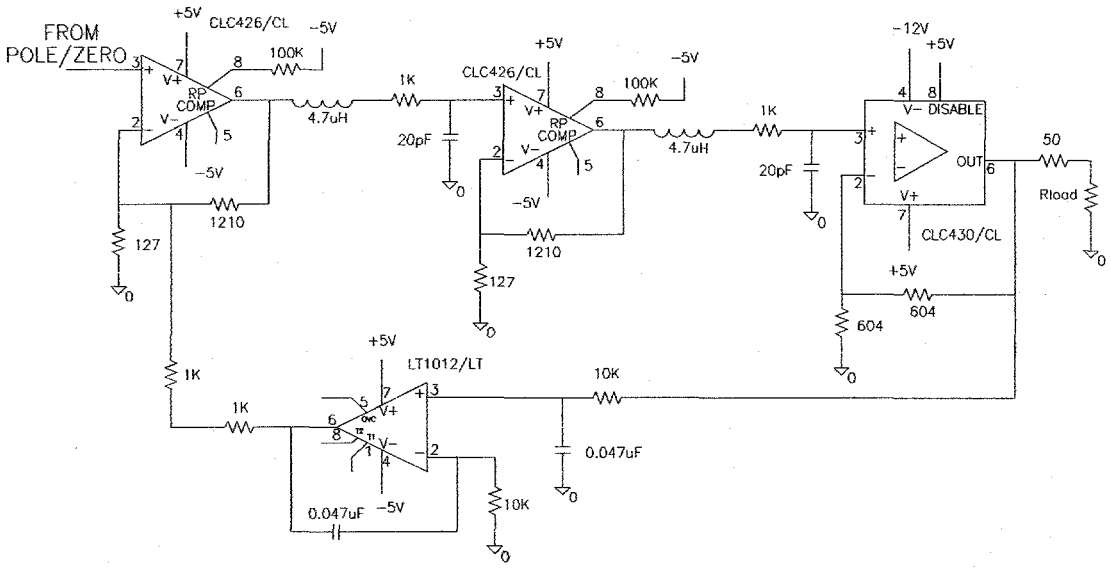

Figure 3
Gain and shaping stages with 100 ns matched filter and output buffer

2.3.1 Noise Results

The results are shown in **Figures 9** and **10** comparing the simulated results to measured results.

2.3.2 AC Analysis Results

The small signal analysis results are shown in **Figure 4**. The results shown here indicate a bandwidth of about 6.5 MHz with a lower frequency cutoff of about 3 kHz.

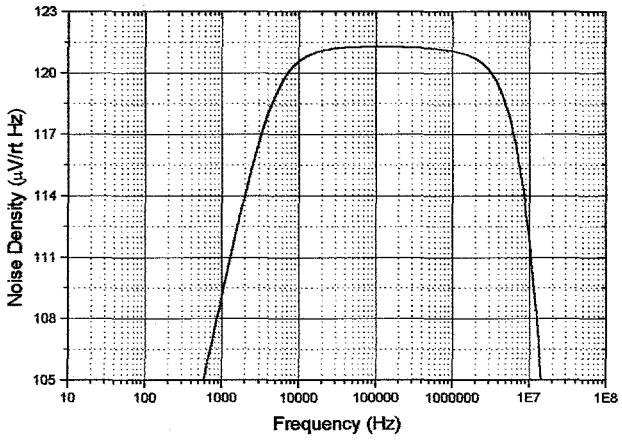

Figure 4
Small signal simulation results

2.3.3 Transient Analysis Results

Simulation results are shown here for 100 ns (**Figure 5**) and 400 ns (**Figure 7**) pulses and the baseline recovery at a rate of 10 kHz (**Figure 6** and **Figure 8**).

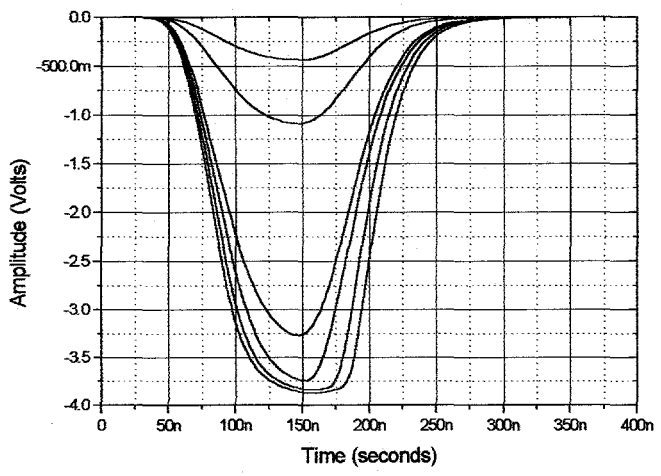

Figure 5
Response for 100 ns current pulses

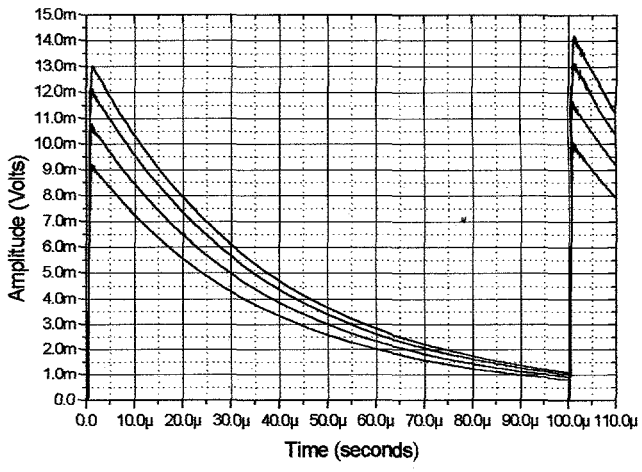

Figure 6
Baseline for large signal inputs (PRR of 10 kHz)

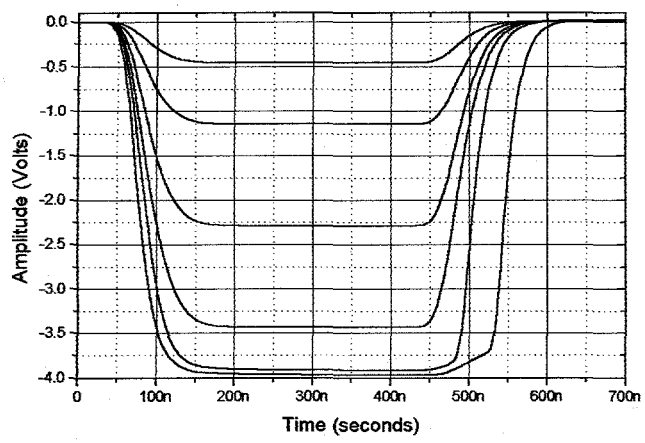

Figure 7
Response for 400 ns current pulses

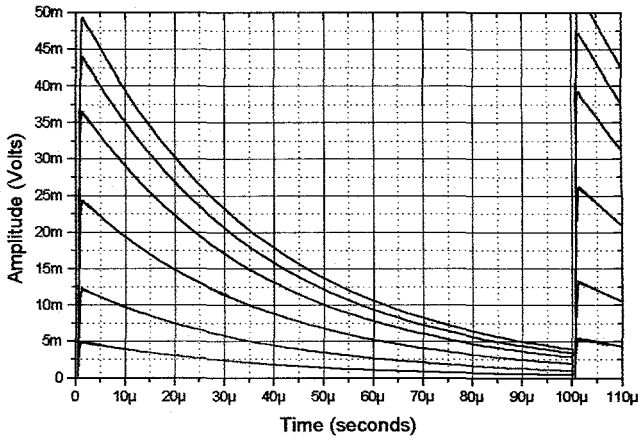

Figure 8
Baseline for large signal inputs (PRR of 10 kHz)

3. PERFORMANCE

3.1 Amplifier (no detector load, 300 K)

Measurements were made on the amplifier using the oscilloscope and a spectrum analyzer to determine the noise levels, AC performance, and transient performance. These tests were performed with the amplifier setup as it would be with the detector with the exception that the front-end electronics is at room temperature and no detector load is simulated (capacitive load). For the transient measurements, the parasitic capacitance (0.1 pF to 0.2 pF) of a 1 GΩ resistor was used to generate a current pulse from a voltage ramp, (impulse, 100 ns, 400 ns). For the spectrum analyzer measurements, a 200 kΩ resistor was used to input the current signal. This would increase the noise, but the signal injected was above the noise level and in addition no front end load was used during the noise measurements.

3.1.1 Noise Performance

The measured and simulated noise spectral densities (into 50 Ω) are shown in **Figure 9**. The integrated noise measured at the output of the amplifier was 2.8 mV rms (into 50 Ω) with the front-end FET at room temperature.

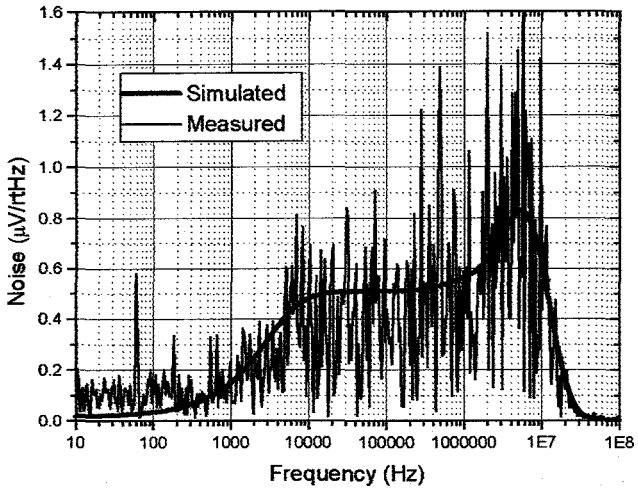

Figure 9
Noise spectral density of amplifier into 50 Ω, JFET at 300 K, no detector load

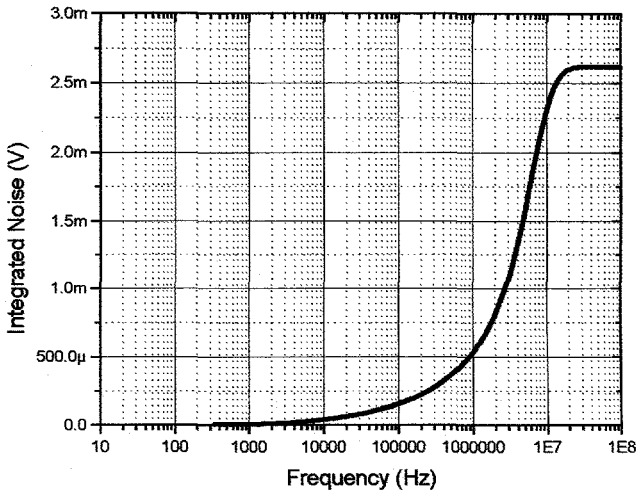

Figure 10
Simulated integrated noise, into 50 Ω, JFET at 300 K, no detector load, the measured rms noise was 2.6 mV

3.1.2 AC (spectrum) measurements

Figures 11 and **12** show the spectrum analyzer measurements over a 50 dbm range. **Figure 11** shows the output in 10 dbm steps. **Figure 12** shows the output in 2 dbm steps. The bandwidth for all amplitudes is almost constant, about 4 MHz. The bandwidth is marked on each curve.

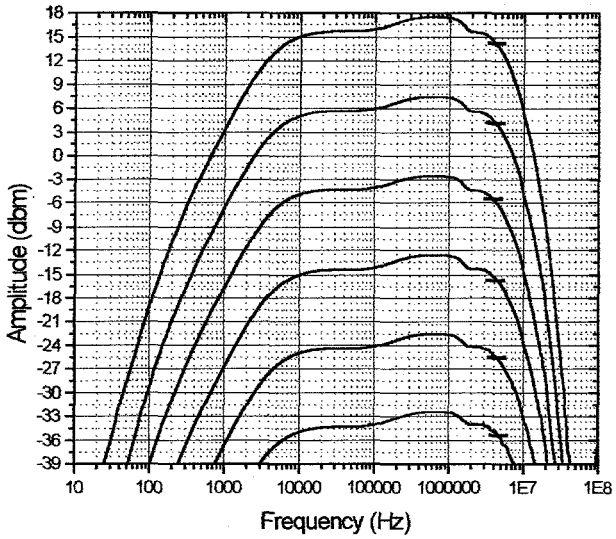

Figure 11
Spectrum analyzer plots from amplifier into 50Ω, 10 dbm/step

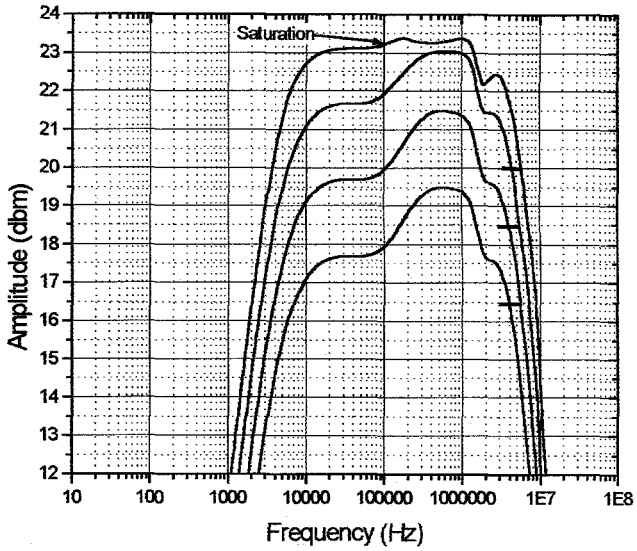

Figure 12
Spectrum analyzer plots from amplifier into 50Ω, 2 dbm/step

3.1.3 Transient measurements

The results from a 10 ns pulse (impulse) are shown in **Figure 13**. The results for 100 ns pulses are shown in **Figure 14, 15, 16 and 17**. The response is very similar to the simulation results. The baseline recovery time for the measured signals was better than the simulation.

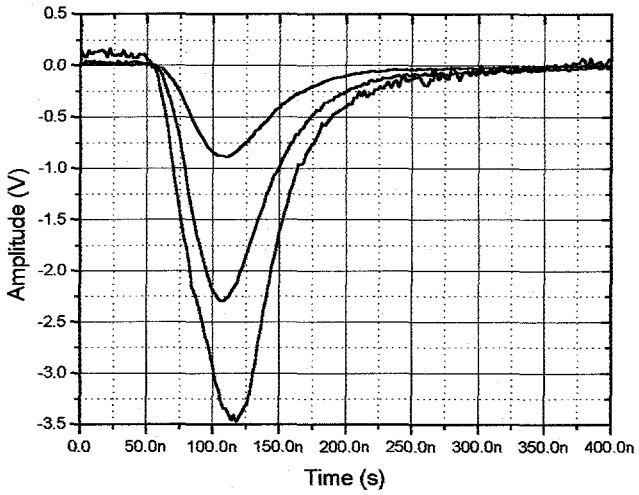

Figure 13
Impulse response from 10 ns pulse input to amplifier

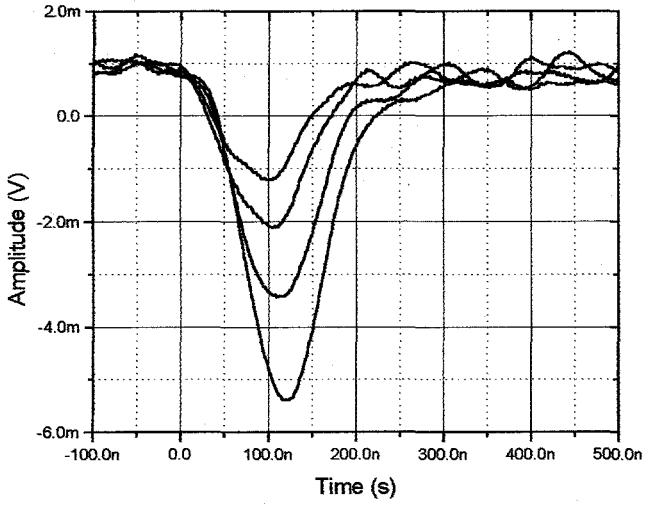

Figure 14
Response to 100 ns pulse input, small signal response

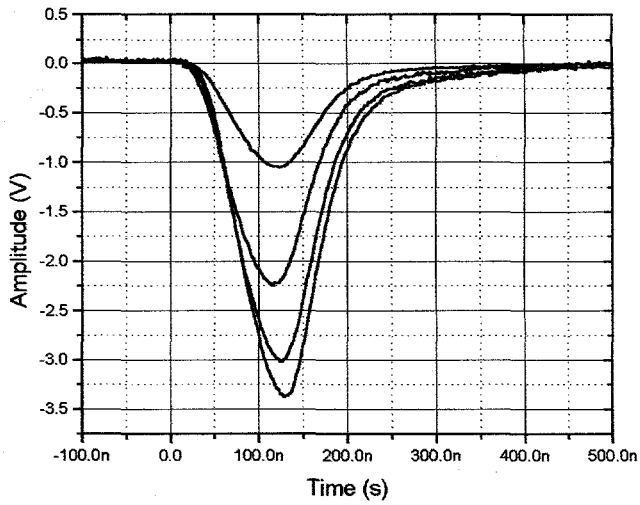

Figure 15
Response to 100 ns pulse input, large signal response

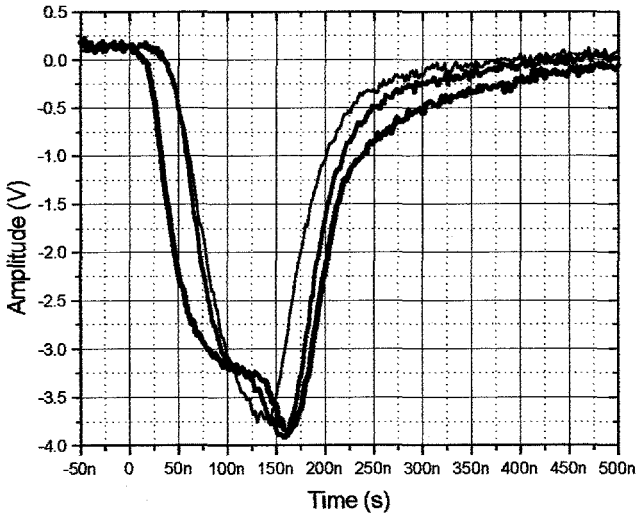

Figure 16
Large input signal response, signals showing distortion from saturation

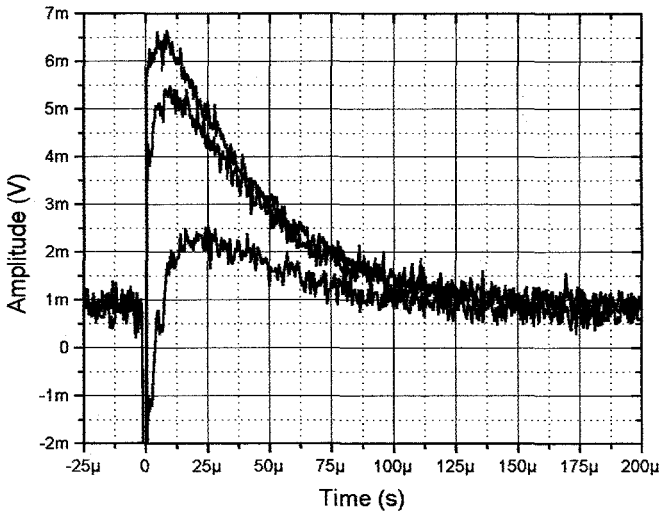

Figure 17
Baseline recovery from large input signals

The results for 400 ns pulses are shown in **Figures 18**, **19**, **20**, and **21**. The baseline recovery for large signals are significantly longer and amplitude is larger than indicated by simulations. This effect was not seen with the detector. The detector is nonlinear and will not show the same behavior as the experimental setup.

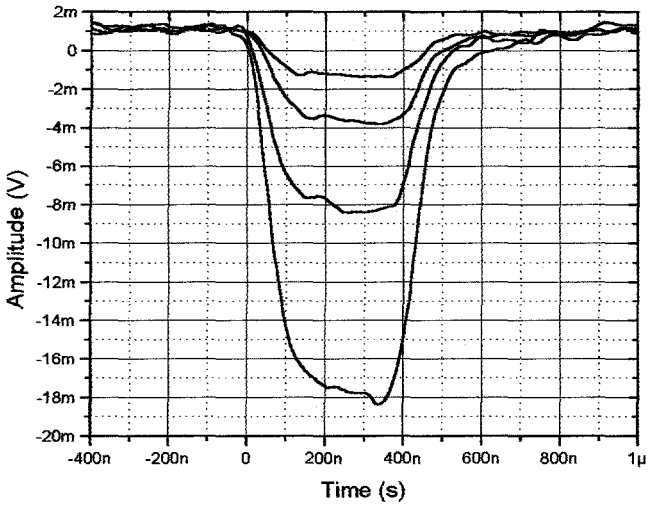

Figure 18
Response to 400 ns pulse, small signal

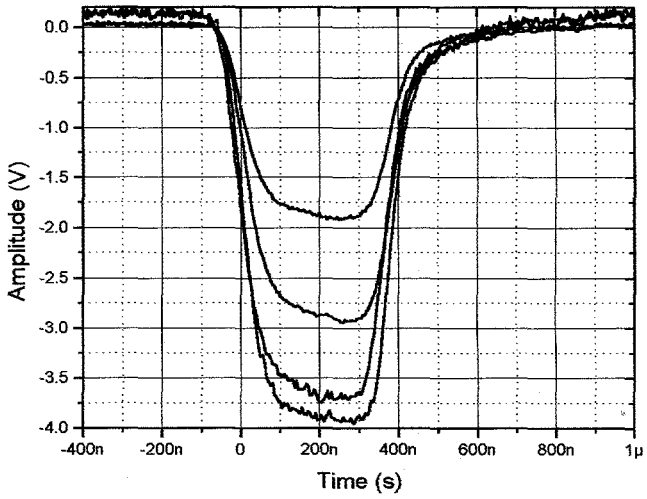

Figure 19
Response to 400 ns pulse, large signal

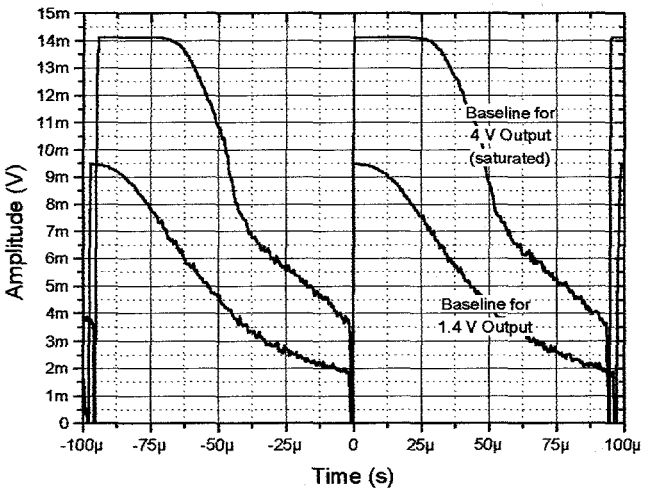

Figure 20
Baseline recovery for two large signals at 10 kHz rate

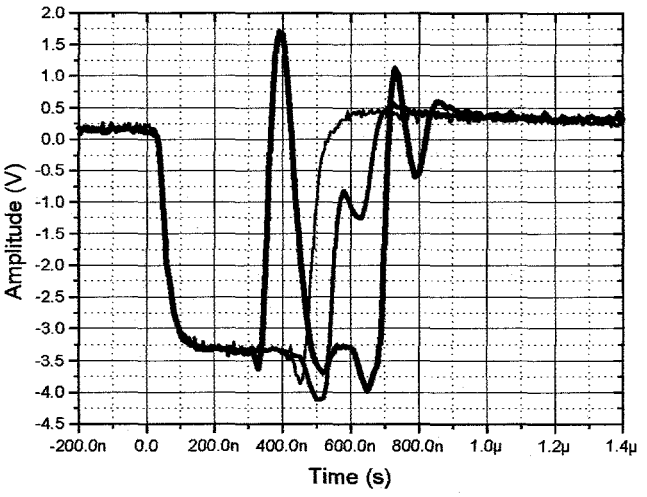

Figure 21
Response to overdriving the amplifier with 400 ns pulses

3.2 Detector and amplifier system

The following results show the performance of the integrated detector/amplifier receiver system. The measurements show the performance with the detector operating at about 25 K, (unless specified otherwise), and the front-end electronics (JFET, feedback components, detector bias resistors and capacitors) operating at about 140 K. The mechanical cryopump is operating through all tests unless otherwise indicated.

3.2.1 Noise Performance

The noise spectral density is shown for a 77 K Black Body (BB) source with integrated noise of about 4 mV (**Figure 22**), a 300 K background radiation source with integrated noise of about 7.8 mV (**Figure 23**), a 300 K BB source with optical bandwidth of 8.6 μm to 11.6 μm with integrated noise of about 5.8 mV (**Figure 24**), and a 300 K BB source with optical bandwidth of 9.2 μm to 12.7 μm with integrated noise of about 6.4 mV (**Figure 25**).

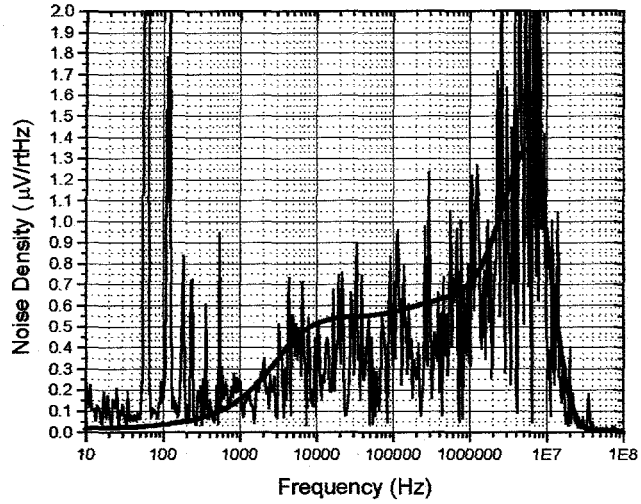

Figure 22
Amplifier/Detector noise spectral density and simulated noise spectral density with 20 pF load and JFET at 140 K. The detector is looking into a 77 K BB source

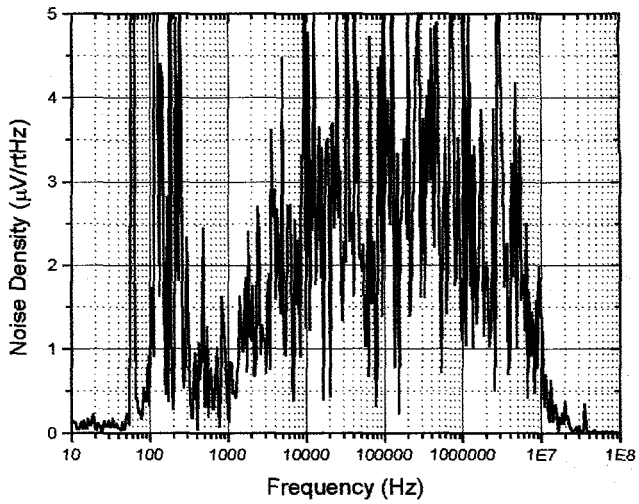

Figure23
Amplifier/detector noise spectral density with the detector looking into a 300 K background radiation source (no optical filter)

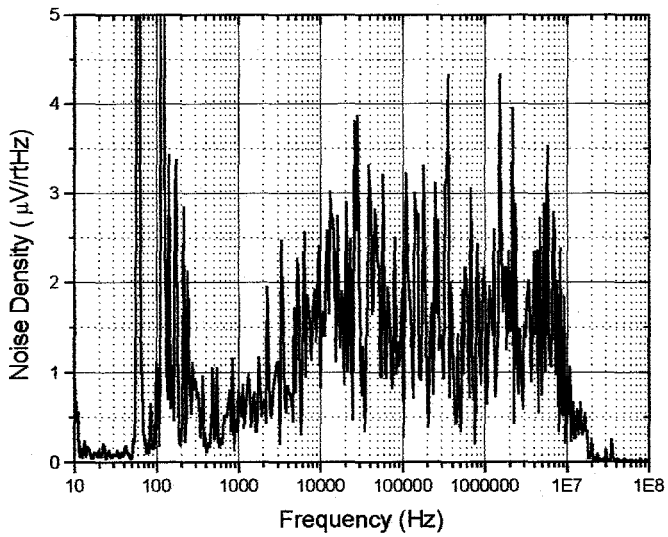

Figure 24
Amplifier/Detector noise spectral density with the detector looking at a 300 K BB source through an optical bandpass filter, 8.6 μm to 11.6 μm

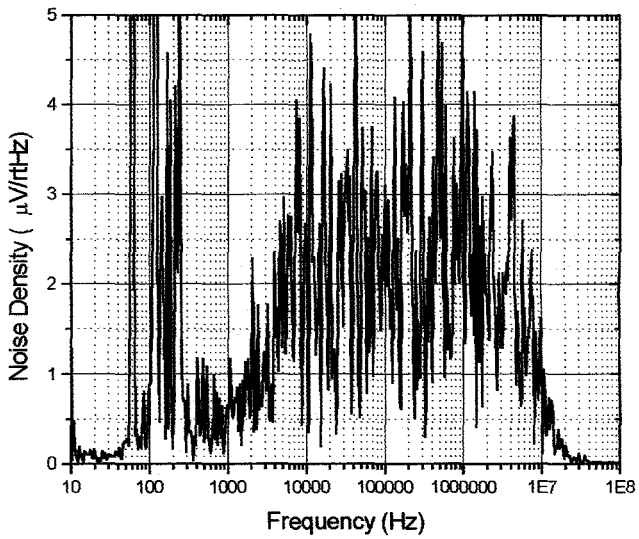

Figure 25
Amplifier/Detector noise spectral density with the detector looking at a 300 K BB source through an optical bandpass filter, 9.2 μm to 12.7 μm

3.2.2 Laser impulse measurements

The receiver system was driven by a pulsed CO_2 laser scattering. The laser pulse width was about 18 ns. The responses are shown in **Figures 26** and **27**. Final integration of receiver and laser is currently underway. The integrated test results were not available at this writing.

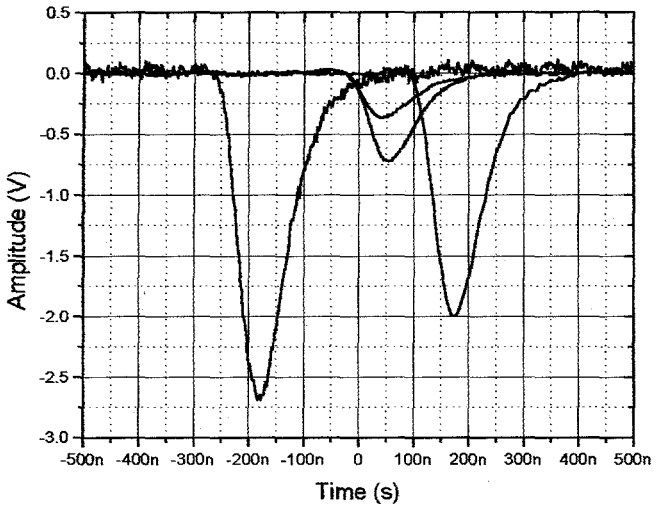

Figure 26
Examples of the detector amplifier response to a CO_2 laser pulse of width 18 ns scattered off the surroundings

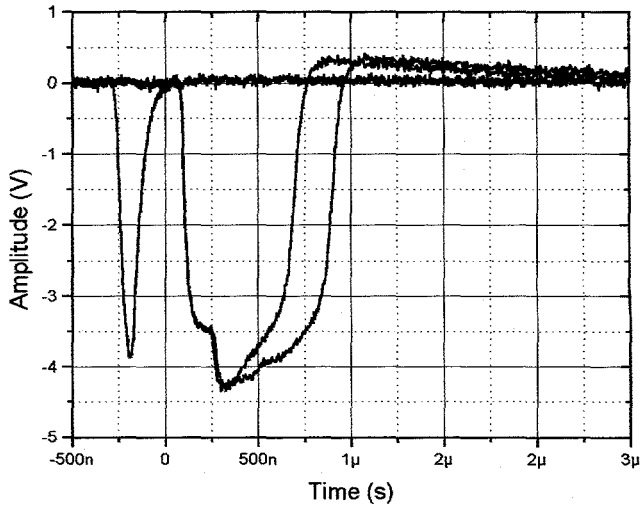

Figure 27
Examples of saturation recovery time from overdriving the detector and amplifier with large signal scatter from a CO_2 laser

4. CONCLUSION

A background-limited (low-noise), high-bandwidth detector/amplifier system with 1/f rejection has been designed and tested. The measured results were very similar to the simulated results. The system is optimized for 100 ns pulses with a minimum detectable current amplitude of 4 nA and a maximum amplitude of 4 µA, for a dynamic range of 60 db. The active detector bias will sink up to 20 µA of photocurrent while maintaining a stable bias. The noise is minimized by the cooling of the front-end FET and by reducing the lengths of the detector/amplifier interconnects which are kept short by mounting the critical front-end components inside the dewar with the detector. The active baseline restoration circuit minimizes drift and correlated 1/f noise for optimal pulse averaging.

5. REFERENCES

1. Bradly J. Cooke, Mark Schmitt, Roy M. Goeller, Steve Czuchlewski, Kenneth Fuller, Nicholas Olivas, Bryan Laubscher and Robert Sander, "CO_2 DIAL Transmitter/Receiver Noise Characterization and Related Correlated Noise Issues," *Proc. SPIE, Gas and Chemical Lasers*, pp.2-15, Feb. 1996

2. E. L Dereniak, G. D. Boreman, *Infrared Detectors and Systems,* pp.168-185, John Wiley and Sons, Inc., New York, 1996

3. Paul R. Gray, Robert G. Meyer, *Analog Integrated Circuits,* pp.635-677, John Wiley and Sons, Inc., New York, 1984

4. Bradly J. Cooke, "PV Detection and Transimpedance Amplification Response and Noise," *Mathcad paper,* unpublished, 1995

5. Ferrel G. Stremler, *Introduction to Communication Systems,* pp. 406-412, Addison-Wesley Publishing Company, Inc. 1982

6. Bradly J. Cooke, Bryan E. Laubscher, Maureen Cafferty, Nicholas L. Olivas, Mark J. Schmitt, Kenneth R. Fuller, Roy M. Goeller, Donald E. Mietz, Joe J. Tiee, Robert K. Sander, John L. Vampola, Stephen L. Price, and Ichiro Kasai, "Analysis and Design Methodology for the Development of Optimized, Direct-Detection CO_2 DIAL Receivers," *Proc. SPIE, Infrared Instrumentation,* July 97

7. Paul Hendriks, "High-Speed, Low-Distortion Tunable Bandpass Filter", *Electronic Design, Analog Applications Issue,* pp. 63-64, November 20, 1995